



Visible light photocatalysis of Methylene blue by graphene-based ZnO and Ag/AgCl nanocomposites

M. Vanitha, Keerthi, S. Vadivel, N. Balasubramanian*

Department of Chemical Engineering, A.C. Tech Campus, Anna University, Chennai, India, Tel. +91 44 22359190, +91 9444954151; email: nbsbala@annauniv.edu

Received 12 September 2013; Accepted 5 March 2014

ABSTRACT

The present investigation deals with the photocatalytic activity of two different graphene oxide-(GO) based nanocomposites i.e. Ag/AgCl/GO and ZnO/GO for the degradation of Methylene blue (MB). The composites were prepared by low-temperature hydrothermal method and were characterized using scanning electron microscope (SEM), X-ray diffraction (XRD), and Raman spectroscopy. SEM analysis showed that GO was stacked between the hexagonal ZnO nanostructures and in the case of Ag/AgCl, it was grafted onto the distorted spheres of Ag/AgCl. This distorted structure may be due to the overloading of the silver precursor close to the saturation during the synthesis. XRD pattern confirms the formation of both the nanocomposites. Both the nanocomposites showed good performance in degrading the dye under sunlight. ZnO/GO being a semiconductor photocatalyst showed 95% removal of dye in 100 min, whereas plasmonic catalyst Ag/AgCl/GO was found to degrade 92% of MB within 50 min of reaction time due to its unique surface plasmon resonance property. Raman spectroscopy confirms the enhanced photocatalytic activity of both the nanocomposites, which is due to the electron-accepting property of the GO and hinders the recombination of electron–hole pair.

Keywords: Methylene blue; Visible light; Graphene; Surface plasmon resonance; Photocatalyst

1. Introduction

Industries, such as textile, refineries, chemical, plastic, and food-processing plants produce wastewaters characterized by a perceptible content of organics. Textile wastewater is known to exhibit strong color, large amount of suspended solids, fluctuating pH, temperature, and high-chemical oxygen demand concentration. The main pollutants in textile wastewater originate from the dyeing and finishing steps. Textile industries cause serious environmental problems

because of the toxic wastewater produced. Conventionally biological treatment, chemical precipitation, adsorption, and membrane technology are adopted to treat textile effluent. However, due to low biodegradability, toxicity, and strong color, the conventional methods fail to treat the textile effluent to the satisfactory level of pollution control board norms. Because of increased environmental pressures to adopt a better technology for treating organic effluent, industries are trying various alternative processes to aspire to “zero discharge” [1]. Photocatalysis is gaining a lot of attention in the area of purification, such as degradation of organic pollutant, dyes in water with the use

*Corresponding author.

of sunlight as the energy source, and atmospheric oxygen as an oxidant, which accelerates light-driven chemical reactions. Photocatalysts achieve their importance due to captivating properties, such as quantum confinement and enhanced reactivity.

Graphene has received great attention with diversity in its application in nanoelectronics, catalysis, batteries, sensors, and supercapacitors [2]. This is due to its novel one-atom-thick two-dimensional (2-D) graphitic carbon system and magnificent mechanical, electrical, thermal, and optical properties [3]. Graphene has the perfect sp^2 hybrid carbon nanostructure and higher specific surface area when compared to other carbon forms. There are various synthesis routes from natural graphite by chemical oxidation and electrochemical exfoliation. Alternatively it can be produced by reduction of graphene oxide (GO) by various reducing agents [4]. But the reduction of GO may not lead to the complete removal of oxygen containing functional groups, and hence, it renders a surface with good dispersion property and acts as an anchoring site for supporting metal oxide nanoparticles. GO may tend to restack leading to the reformation of precursor and metal oxides tend to agglomerate forming lumps/clusters, which affects its efficiency in wider applications. The union of GO and metal oxide nanocomposites eliminates the barriers which restrict its application individually. Many metal oxides have been used to deposit on the GO and the resultant composite exhibits finer photocatalytic properties [5].

Diverse photocatalytic materials have been used for dye degradation, including TiO_2 , ZnO, Ag/AgCl, CdS, Fe_3O_4 , SnO_2 , V_2O_5 , and WO_3 [6–10]. Among them, ZnO is inexpensive and non-toxic [11] and Ag/AgCl shows efficient photocatalytic activity in the visible region due to their plasmon resonance effect [12]. Zinc oxide (ZnO), an *n*-type semiconductor has a wide band gap of 3.37 eV, with high photosensitivity [13], which when exposed to sunlight yields photoelectrons and holes and these photoelectrons are utilized for dye degradation [14]. Whereas Ag/AgCl has boosted photocatalytic activity due to an efficient charge separation/transfer and hence is a competent visible light-triggered plasmonic photocatalyst.

GO has large surface area with reactive oxygen functional groups on its surface which makes it a good matrix for supporting metal or metal oxide/halide nanoparticles. It enjoys the candidature as a catalyst carrier/promoter due to the property of high chemical and thermal stability with locally conjugated aromatic system [15,16]. Clubbing of GO with ZnO, i.e. ZnO/GO nanocomposite, has shown good photocatalytic performance owing to the reduction of the

recombination of charge carriers on the catalysts surface leading to structural changes, required for an efficient photocatalyst [17]. Similarly, GO plays a vital role in supporting the development of visible light-energized photocatalysts, such as Ag/AgCl. The hybridization of nanocomposites with GO is expected to satisfy the three aspects of effective photodegradation i.e. (1) effective transfer of photoelectrons to significantly hamper the recombination of photoelectrons and holes; (2) a suitable substrate which immobilize and support catalyst; and (3) a superior absorption capacity of the catalytic system towards the dye or pollutants [18,19].

This work discusses the hydrothermal synthesis of ZnO/GO and Ag/AgCl/GO under low-temperature conditions, involving mild reducing agents. The present work investigates the performance of semiconductor photocatalyst and light-activated plasmon resonance catalyst for the photocatalytic degradation of Methylene blue (MB) under visible light.

2. Materials and methods

2.1. Materials

Silver nitrate ($AgNO_3$), zinc nitrate ($Zn(NO_3)_2$), potassium permanganate ($KMnO_4$), sulfuric acid (H_2SO_4), graphite powder, cetyl tetra ammonium bromide (CTAB), sodium hydroxide (NaOH), and hydrogen peroxide (H_2O_2) were used as received without further treatments.

2.2. Synthesis of GO

GO was synthesized by chemical exfoliation of graphite powder using a modified Hummers' method. The synthesis procedure was carried out according to the methods described earlier [20].

2.3. Synthesis of Ag/AgCl/GO nanocomposite

Ag/AgCl/GO nanocomposite is synthesized by hydrothermal method involving the following steps. In the first step, Ag/GO was synthesized from GO and $AgNO_3$ precursors. An aqueous solution of GO was obtained by sonicating 40 mg of GO in DI water for 1 h to acquire a stable homogenous suspension of brown-colored GO solution. Silver-ammonia complex was prepared from 0.1 M $AgNO_3$ and 3 M ammonia solutions and GO suspension were added and stirred for 30 min to develop a homogenous solution and 0.3 M glucose solution was added. The solution was left undisturbed for nearly 1 h at room temperature to allow the nucleation process and was heated at 40°C

for 3 h. Then the autoclave was cooled to room temperature and the product was washed repeatedly with ethanol water mixture to remove any impurities, and the products were dispersed in 100 ml of water. The Ag/GO dispersion was used as the precursor for the synthesis of Ag/AgCl/GO, 80 ml of FeCl₃ solution was added dropwise and stirred at room temperature for 2 h, after which the resulting precipitate was washed with deionized water and dried at room temperature and used for further characterization. Ag/AgCl was synthesized in a similar way without the addition of GO.

2.4. Synthesis of ZnO/GO nanocomposite

ZnO/GO nanocomposite is synthesized by the following procedure. A 50 ml of Zn(NO₃)₂ (0.2 mol) was stirred vigorously with 0.5 g of CTAB for 1 h. Then, GO (0.40 g) was dissolved in 50 ml of deionized water and sonicated for 1 h to exfoliate the GO to obtain a brown solution. Subsequently, GO suspension was added into the Zn(NO₃)₂ aqueous solution and stirred for nearly 0.5 h, followed by the addition of 0.3 mol of NaOH solution dropwise till the pH rose to 11. The reaction mixture was stirred for another 30 min to allow the growth process of the particles and then subjected to heating in a pressurized condition for 10 h at 90 °C in a muffle furnace. The resultant product was cooled to room temperature and centrifuged several times with distilled water at 3,000 rpm and dried at 60 °C for 5 h under vacuum. The resultant product contains zinc in its hydroxide form, and hence, it is subjected to calcination at 500 °C for 2 h to obtain ZnO/GO nanocomposite and is characterized. Bare ZnO was synthesized without the addition of GO by the same procedure mentioned above.

2.5. Characterization

The scanning electron microscope (SEM) images were obtained using SEM (FEI Quanta FEG 200), USA. X-ray diffraction (XRD) analysis was performed using an X-ray diffractometer (Xpert Pro, Pan Analytica) with Cu K α radiation ($\lambda = 1.5418$ Å). The Raman spectra were recorded on a Renishaw in Via plus Raman microscope using a 532 nm excitation laser. The photodegradation of the MB dye was monitored by measuring the real-time UV–vis absorption of MB at 664 nm using a JASCO UV-550 spectrometer.

2.6 Photocatalysis

For photocatalytic reaction, 5 ml (10 mg/ml) of dispersed suspension of the as-synthesized nanostruc-

tures was transferred to a 200 ml beaker containing 45 ml aqueous solution of MB (10 mg/l). The dispersion was kept in the dark for 30 min so that the dye molecules and catalysts achieve equilibrium after which the degradation was accomplished in sunlight. A 2 ml of dye solution was taken at regular intervals, centrifuged, and the absorbance was recorded using a UV–vis spectrophotometer (Shimadzu 1800) at 664 nm.

3. Results and discussion

SEM images of the synthesized GO and the composites containing GO with ZnO and Ag/AgCl are shown in Fig. 1(a)–(c), respectively, to exemplify the morphological information. It can be observed from the figure that the GO sheets appear as crumpled silk veil waves, with stacking of the sheets leading to a multilayered structure. The SEM image also conveys that the GO sheets are transparent and exhibit a larger surface area which allows further modifications [21]. It can be noted that nanoparticles in the range of 500 nm were obtained in the case of Ag/AgCl/GO nanocomposite as exposed in Fig. 1(b). The micrograph of Ag/AgCl/GO composite exhibits some aggregation of AgNPs owing to the elevated loading of the precursor close to saturation [20]. In order to confirm whether the AgNPs is grafted on to the GO surface, it was further characterized by Raman spectra and XRD analysis. SEM analysis of the ZnO-based GO composite in Fig. 1(c) confirms the wurtzite structure of ZnO nanoparticles with a hexagonal structure. The figure also illustrates that ZnO is enwrapped tightly with the GO surface indicating the strong relationship between them [22] favoring its performance as a photocatalyst. The strong interaction may be due to the presence of functional groups in the GO moieties.

One of the most significant tools used to characterize sp² and sp³ hybridized carbon atoms and to discriminate the disorder/defect structures is the Raman spectroscopy [23] and it is considered to be the fingerprint for carbon-based materials. Transfer of charge between GO and the hybridized material could also be verified by the Raman spectra. The characteristic peaks of GO and Ag/AgCl/GO are shown in Fig. 2(a). The G band in GO corresponds to the E_{2g} mode, and the D band corresponds to the k-point phonons with A_{1g} symmetry mode for sp² carbon atoms. The intensity ratio of D band to the G band is the measure of disorder/defects in the graphene; a decrease in the intensity ratio indicates the less defective nature of the graphitic crystal domains [24]. The I_D/I_G ratio of GO (0.8418) is slightly lower when compared to the Ag/AgCl/GO (0.8458) which may be due to the defects in the GO

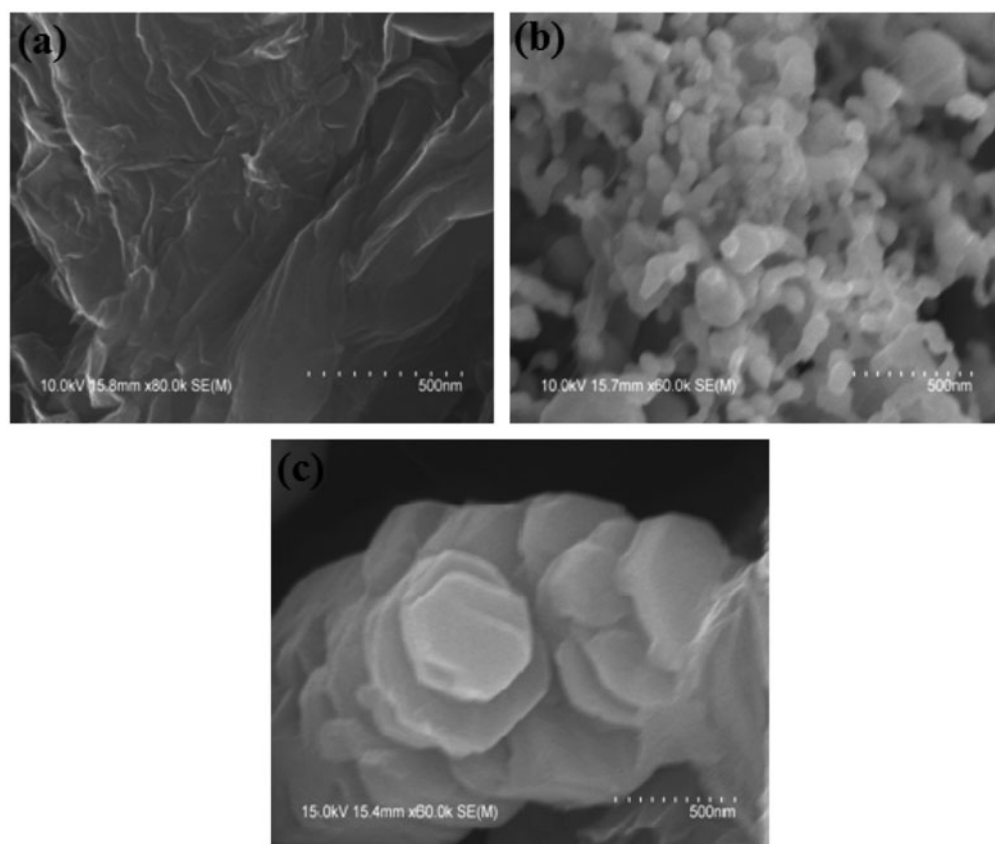


Fig. 1. SEM micrographs of (a) GO, (b) Ag/AgCl/GO, and (c) ZnO/GO.

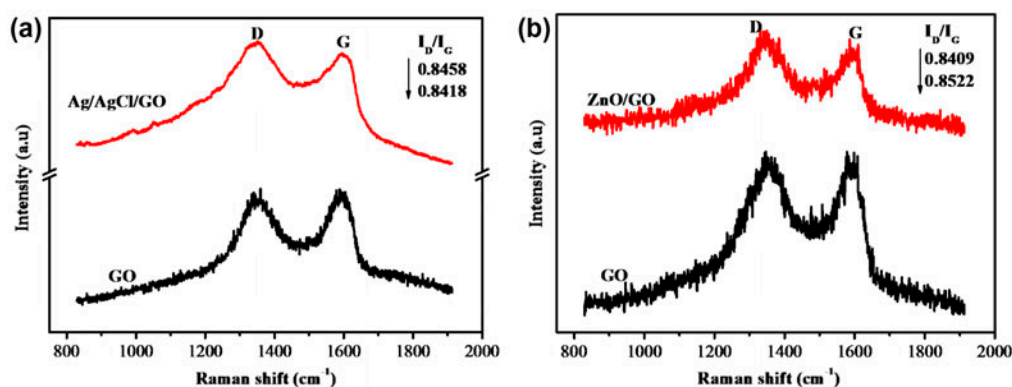


Fig. 2. Raman spectra of (a) plasmonic Ag/AgCl/GO and (b) ZnO/GO nanocomposite prepared at low temperature.

synthesized by Hummer's method. The red shift of the D band from 1,357/cm in GO to 1,346/cm in Ag/AgCl/GO suggests that the reduction of GO has occurred and shift of G band to lower frequency at 1,587/cm for Ag/AgCl/GO nanocomposite, compared to 1,595/cm of GO, intimates that GO has been hybridized with the electron donor component itself acting as an acceptor [25]. Fig. 2(b) shows the Raman

spectra of GO and ZnO/GO nanocomposite. The G band shifts from 1,595/cm in bare GO to 1,590/cm in the case of ZnO/GO nanocomposite supporting the hybridization of GO with the electron-donor component. The I_D/I_G ratio of GO (0.8483) is slightly higher when compared to the ZnO/GO (0.8409), indicating the smaller particle size of the synthesized nanocomposites.

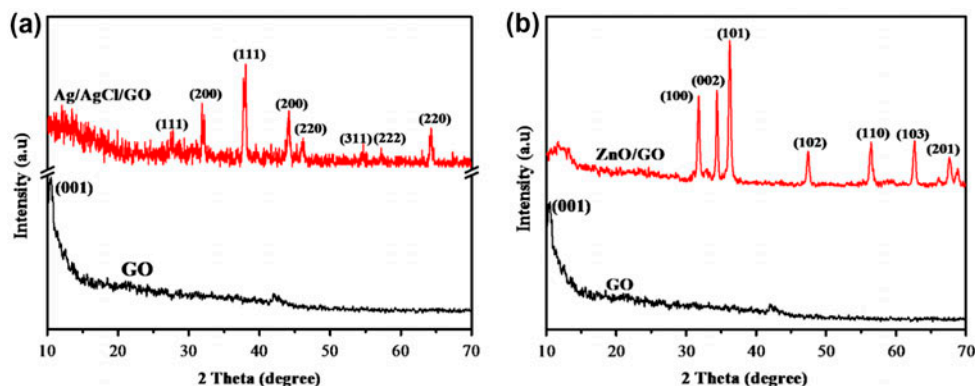


Fig. 3. XRD pattern of (a) plasmonic Ag/AgCl/GO and (b) ZnO/GO nanocomposite synthesized by hydrothermal method.

XRD studies were used to examine the structural changes originating from the oxidation of graphite to GO and also the formation of Ag/AgCl/GO and ZnO/GO nanocomposite by low-temperature hydrothermal synthesis. Fig. 3(a) and (b) show the XRD pattern of GO, which exhibits an intense and sharp peak at 10.46° assigned to (001) plane [26]. The enhanced interplanar distance of GO when compared to the pristine graphite which displays its characteristic peak at nearly 26° with (002) plane [27] is because of the intercalated oxygen-containing functional groups in GO. Fig. 3(a) displays the XRD pattern of Ag/AgCl/GO photocatalyst synthesized using mild reducing agent and was investigated to examine the formation of Ag/AgCl/GO nanocomposite. The individual diffraction peaks at 2θ values of 38.04° (111), 44.12° (200), and 77.27° (420), correspond to the cubic phase of metallic Ag (JCPDS card No. 65-2871) which signals the existence of Ag⁰ in the composite. Similarly, peaks at 64.08° (220), 27.76° (111), 31.89° (200), 46.10° (220), 54.56° (311), and 57.32° (222), are indexed to the AgCl (JCPDS card No. 31-1238) cubic phase [28]. Apart from the cubic-phased metallic Ag and AgCl, there are no diffraction peaks analogous to other impurities which were observed, suggesting that the synthesized nanocomposite contains metallic Ag and AgCl in cubic phase [29]. However, it can be confirmed from the figure that there are no discriminate peaks for GO in the composite [30], which may be possible due to the veiling of the GO signals by the stronger Ag signals. Another reason for the weak signal peak of GO in the Ag/AgCl/GO nanocomposite may be due to more eminent exfoliation of GO on the subsequent formation of AgNPs in the composite [31] which can also be affirmed by the XRD analysis.

The synthesized ZnO/GO composite exhibits peaks at 2θ values at 31.7° , 34.4° , 36.16° , 47.36° , 56.44° ,

62.52° , 66.04° , and 68.8° corresponding to the crystal planes of (100), (002), (101), (102), (110), (103), (201), and (200) [32], respectively, as illustrated in Fig. 3(b). All the diffraction peaks of ZnO/GO nanocomposites coincide with the hexagonal wurtzite (JCPDS card No. 36-1451) phase-structured ZnO [33] which are consistent with the JCPDS standard and also are reinstated from the SEM micrograph as shown in Fig. 1(c). The XRD pattern of the ZnO/GO nanocomposite does not reveal any characteristic peaks for impurities, such as zinc hydroxide and graphite. Apart from this, a weaker peak at 11.64° was observed in the composite indicating that GO is not completely reduced to rGO, this may be due to the low temperature and absence of toxic strong reducing agents involved in the synthesis route.

3.1. Comparison of Photocatalytic performance

The photocatalytic degradation performance of ZnO/GO and Ag/AgCl/GO was evaluated on MB dye. Before exposing the dispersed suspension of MB and the photocatalysts in sunlight, it was kept in dark to accomplish the adsorption–desorption equilibrium between the dye and the catalysts. In both the cases of Ag/AgCl/GO and ZnO/GO, the photocatalytic degradation of MB was done under visible light irradiation. The degradation of the dye was monitored using UV–vis absorption spectra and it can be seen from the Fig. 4(a), that 92% of the dye degraded within 50 min time of exposure in the case of the Ag composite. The key factor for an effective photocatalytic activity is the efficient charge separation/transfer by the photocatalyst. Here, GO could promote electron transfer occurring in the photocatalysts acting as catalyst carrier/promoter/co-catalyst

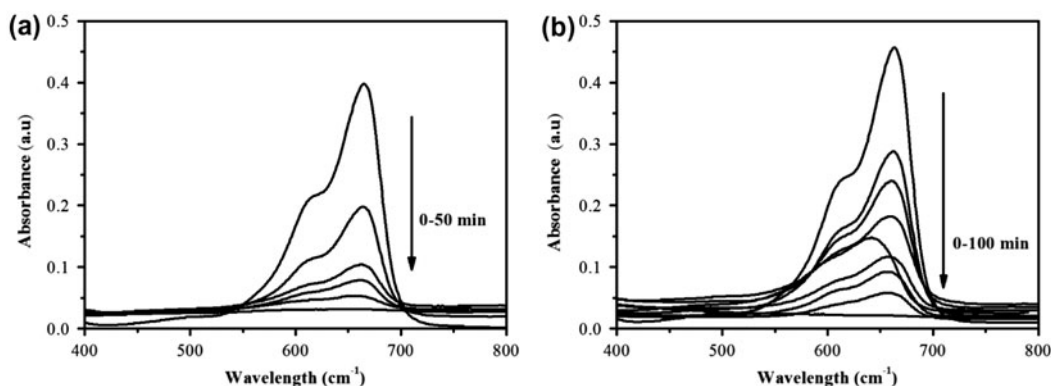


Fig. 4. UV-vis spectrum depicting the decrease in the absorbance of MB using visible light photocatalyst (a) Ag/AgCl/GO and (b) ZnO/GO nanocomposite.

[34]. The increased photocatalytic activity of Ag/AgCl/GO originated from the combined effect of GO, which acts as a co-catalyst with the transmission of photogenerated electrons. On irradiation by sunlight, the Ag/AgCl/GO nanocomposite effectively absorbs the incident photons due to the confined surface plasmon resonance (SPR) excitation of Ag nanoparticles existing in the visible region, reinforcing the separation of photogenerated electron and hole pair. This absorbed photon would be subsequently assorted into an electron and a hole, and the photoelectron of Ag nanocrystals is shifted to the CB (conduction band) of AgCl surface and then to the GO sheets as depicted in Fig. 5(a) [32]. This transference of photoelectrons from AgCl to GO may be due to the presence of an energy band offset between them [35]. These electrons are pinned by oxygen in the reaction system to form various reactive oxygen species and the holes generated by the separation of incident photon are held on the surface of Ag nanocrystals where it oxidizes the dye molecule into various smaller fragments with less toxicity. The hole on the surface of AgCl brings about the oxidation of chloride ions to produce chlorine atoms which are

highly reactive radical species that are responsible for the oxidation of organic molecules, such as dyes [23] as schematically shown in Fig. 5(a). In addition to the larger surface area disclosed by GO, AgCl particles also contribute to substantial surface active sites for the disintegration of organic substrate.

As stated by Luo et al. [36] the visible light absorption of Ag/AgCl is due to the presence of plasmonic absorption of Ag nanocrystals, since AgCl cannot absorb visible light due to the wide band gap of 3.32 eV leading to difficulty in excitation in visible light and also it is found to be unstable under sunlight. The presence of Ag nanoparticles on AgCl enhances the absorption of visible light due to the strong SPR effect. During the dark adsorption experiment, the catalyst showed a very good adsorptive capacity towards MB through non-covalent π - π intermolecular interaction and there is also a strong interaction between the positively charged MB and negatively charged GO surface [37,38]. Hence, there exists a synergistic effect between the Ag nanoparticles, AgCl, and GO leading to a photocatalyst with remarkable stability and efficiency.

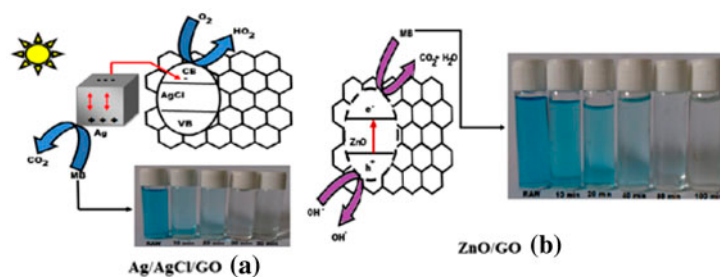


Fig. 5. Schematic representation of the possible mechanism for the degradation of MB using (a) plasmonic Ag/AgCl/GO nanocomposite and (b) ZnO/GO nanocomposite.

The ZnO/GO and dye suspension were exposed to visible light and the concentration changes in the dye were monitored by the absorption profile at 664 nm in UV–vis absorption spectra as shown in Fig. 4(b). The intensity of MB absorbance decreased regularly with the increment in time of exposure, indicating the continuous decrease in MB dye concentration. It was observed that the absorbance of the dye decreases to 95% within 100 min of exposure and the peak in the UV–vis absorption spectra shifted from 664 to 657 nm confirming the structural rupture of the dye during photo degradation. The synthesized composite exhibits enhanced photocatalytic activity for the degradation of MB under both UV and visible light; the present case deals about the degradation of MB using ZnO/GO nanocomposite under visible light irradiation as the former has been discussed widely. The electrons from the CB of ZnO are transferred to the GO surface where it reacts with oxygen to produce superoxide radicals and finally forms highly reactive OH[•] on reaction with electrons of GO leading to the mineralization of MB molecules into CO₂, H₂O, and less toxic minerals [39]. MB molecules are assumed to channelize to the semiconductor surface and get adsorbed via interaction between the dye and the aromatic graphene regions, hence it is suggested that ZnO/GO nanocomposite leads to charge separation, suppressing the recombination of electron and hole pair and adsorption of dyes. The degradation of the MB dye employing ZnO/GO nanocomposite in visible light may be due to the higher adsorption onto the planar structure of GO and π - π interaction between the aromatic ring of the dye molecule and graphene domains as displayed in Fig. 5(b) [40].

The exposure of ZnO/GO nanocomposite to light illumination brings about the photoexcitation of electrons of ZnO which are enhanced by the electronic interaction between GO and ZnO. This causes the electron–hole pair charge separation in ZnO, supported by GO. As GO is a competitive electron acceptor with 2-D π -conjugation structure, it effectively restrains the recombination of photogenerated charge carriers by the transfer of the excited electrons from the CB of ZnO to GO [41]. These photoexcited e⁻ move to the nanocomposite surface and generate reactive oxy radicals, such as superoxide radical ion and hydroxyl radical, which mineralize the dye efficiently [42]. Another possible mechanism for the degradation of dye is the excitation of the dye where it acts as a sensitizer of visible light and throws the electron to GO surface to form the cationic dye radical followed by degradation [43]. GO with various oxygen-containing functional groups permits the absorption of the dye molecule on its surface, where MB is excited and

the electron is transported to the conduction band of ZnO from GO sheets. The surface adsorbed oxygen captures the photoelectron for the generation of the oxidative species which plays a vital role for the degradation of MB [44]. Another important factor for high performance of photocatalysis by the composites may be due to the tight stacking of ZnO nanostructures and GO sheets. GO takes the dual role as electron collector and transporter, crucial factors for the improved photocatalytic behavior under visible light irradiation. The GO sheets are found to be embedded between the hexagonal stacks of ZnO, and hence offer shorter distance for the transference of photoelectrons, which in turn brings enhanced photocatalytic activity towards the dye degradation.

The performance of Ag/AgCl, ZnO, and modified GO nanocomposite photocatalysts were investigated for the degradation of MB (10 mg/l). In the case of bare ZnO, the decline in the dye concentration was only 48%, bare Ag/AgCl resulted in 43% of degradation and in the absence of catalyst there is no considerable degradation as shown in Fig. 6. The modification of GO with Ag/AgCl enhances the activity of the photocatalyst with degradation rate of nearly 92% within 50 min than the bare Ag/AgCl. There is a gradual increase in the photocatalytic behavior of Ag/AgCl/GO nanocomposite with increase in the AgCl content, but due to the instability of AgCl leading to aggregation [37] bare Ag/AgCl shows only 43% degradation. On grafting GO with Ag/AgCl, the degradation rate of MB raised to 92%, where GO being a catalyst carrier with larger surface area prevents the aggregation of Ag/AgCl leading to stability and enhanced photocatalytic performance [20]. The ZnO/GO composite shows enhanced photocatalytic activity than the parent ZnO as the absorption capacity of the

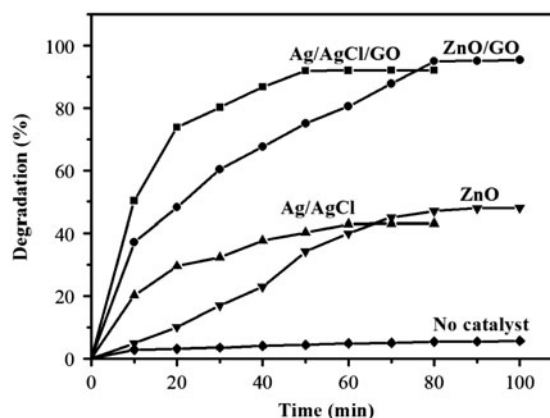


Fig. 6. Percentage degradation of MB towards various catalysts.

composite is high due to the presence of GO with larger surface area, which binds the MB molecules by π - π conjugation with offset face-to-face direction [45].

4. Conclusion

The Ag/AgCl/GO, and ZnO/GO nanocomposites were fabricated via low-temperature hydrothermal process and the photocatalytic performance of the nanocomposite was found to be higher when compared to the Ag/AgCl, and ZnO. The characterization of the synthesized composites using sophisticated instrument confirmed the formation of the GO-based nanocomposites. The comparison of the photocatalytic degradation of MB using ZnO/GO showed 95% removal of dye in 100 min, whereas plasmonic catalyst Ag/AgCl/GO was found to degrade 92% of MB within 50 min of reaction time. The Zn composite showed higher dye degradation at higher process time under visible light since it absorbs visible light only to a small extent. The degradation of MB using ZnO/GO nanocomposite may be due to the higher amount of GO leading to adsorption, whereas silver-based GO composite showed rapid degradation in lesser time due to its unique SPR property.

Acknowledgment

The first author would like to acknowledge the University Grants Commission for providing the fellowship under the basic research scheme.

References

- [1] A. Alinsafi, M. Khemis, M.N. Pons, J.P. Leclerc, A. Yaacoubi, A. Benhammou, A. Nejmeddine, Electrocoagulation of reactive textile dyes and textile wastewater, *Chem. Eng. Process.* 44 (2005) 461–470.
- [2] X.L. Li, X.R. Wang, L. Zhang, S.W. Lee, H.J. Dai, Chemically derived, ultrasmooth graphene nanoribbon semiconductors, *Science* 319 (2008) 1229–1232.
- [3] A.K. Geim, K.S. Novoselov, The rise of graphene, *Nature Mater.* 6 (2007) 183–191.
- [4] S. Stankovich, D.A. Dikin, R.D. Piner, K.A. Kohlhaas, A. Kleinhammes, Y. Jia, Y. Wu, S.T. Nguyen, R.S. Ruoff, Synthesis of graphene-based nanosheets via chemical reduction of exfoliated graphite oxide, *Carbon* 45 (2007) 1558–1565.
- [5] Q. Xiang, J. Yu, M. Jaroniec, Graphene-based semiconductor photocatalysts, *Chem. Soc. Rev.* 41 (2012) 782–796.
- [6] H. Kong, J. Song, J. Jang, Photocatalytic antibacterial capabilities of TiO₂-biocidalpolymer nanocomposites synthesized by a surface-initiated photopolymerization, *Environ. Sci. Technol.* 44 (2010) 5672–5676.
- [7] Z.R. Tian, J.A. Voigt, J. Liu, B. McKenzie, M.J. McDermott, M.A. Rodriguez, H. Konishi, H. Xu, Complex and oriented ZnO nanostructures, *Nature Mater.* 2 (2003) 821–826.
- [8] C. Kim, M. Choi, J. Jang, Nitrogen-doped SiO₂/TiO₂ core/shell nanoparticles as highly efficient visible light photocatalyst, *Catal. Commun.* 11 (2010) 378–382.
- [9] M. Miyauchi, A. Nakajima, T. Watanabe, K. Hashimoto, Photocatalysis and photoinduced hydrophilicity of various metal oxide thin films, *Chem. Mater.* 14 (2002) 2812–2816.
- [10] S.H. Hwang, C. Kim, J. Jang, SnO₂ nanoparticle embedded TiO₂ nanofibers—Highly efficient photocatalyst for the degradation of rhodamine B, *Catal. Commun.* 12 (2011) 1037–1041.
- [11] S. Ameen, M.S. Akhtar, Y.S. Kim, O.B. Yang, H.S. Shin, Synthesis and characterization of novel poly(1-naphthylamine)/zinc oxide nanocomposites: Application in catalytic degradation of methylene blue dye, *Colloid. Polym. Sci.* 288 (2010) 1633–1638.
- [12] J.F. Guo, B. Ma, A. Yin, K. Fan, W.L. Dai, Highly stable and efficient Ag/AgCl@TiO₂ photocatalyst: Preparation, characterization, and application in the treatment of aqueous hazardous pollutants, *J. Hazard. Mater.* 211–212 (2012) 77–82.
- [13] H. Wang, J. Gao, T. Guo, R. Wang, J. Li, Facile synthesis of AgBr nanoplates with exposed {111} facets and enhanced photocatalytic properties, *Chem. Commun.* 48 (2011) 275–277.
- [14] A. Rezaee, H. Masoumbaigi, R.D.C. Soltani, A.R. Khataee, S. Hashemiyani, Photocatalytic decolorization of methylene blue using immobilized ZnO nanoparticles prepared by solution combustion method, *Desalination. Water Treat.* 44 (2012) 174–179.
- [15] B.J. Li, H.Q. Cao, ZnO@graphene composite with enhanced performance for the removal of dye from water, *J. Mater. Chem.* 21 (2011) 3346–3349.
- [16] P.V. Kamat, Graphene-based nanoassemblies for energy conversion, *J. Phys. Chem. Lett.* 2 (2011) 242–251.
- [17] K. Lü, G. Zhao, X. Wang, A brief review of graphene-based material synthesis and its application in environmental pollution management, *Chin. Sci. Bull.* 57 (2012) 1223–1234.
- [18] Y. Liu, Y. Hu, M. Zhou, H. Qian, X. Hu, Microwave-assisted non-aqueous route to deposit well-dispersed ZnO nanocrystals on reduced graphene oxide sheets with improved photoactivity for the decolorization of dyes under visible light, *Appl. Catal. B Environ.* 125 (2012) 425–431.
- [19] G.D. Jiang, Z.F. Lin, C. Chen, L.H. Zhu, Q. Chang, N. Wang, W. Wei, H.Q. Tang, TiO₂ nanoparticles assembled on graphene oxide nanosheets with high photocatalytic activity for removal of pollutants, *Carbon* 49 (2011) 2693–2701.
- [20] M. Zhu, P. Chen, M. Liu, Graphene oxide enwrapped Ag/AgX (X = Br, Cl) nanocomposite as a highly efficient visible-light plasmonic photocatalyst, *ACS Nano* 5 (2011) 4529–4536.
- [21] D. Du, L.M. Wang, Y.Y. Shao, J. Wang, M.H. Engelhard, Y.H. Lin, Functionalized graphene oxide as a nanocarrier in a multienzyme labeling amplification strategy for ultrasensitive electrochemical immunoassay of phosphorylated p53 (S392), *Anal. Chem.* 83 (2011) 746–752.

- [22] S. Stankovich, D.A. Dikin, R.D. Piner, K.A. Kohlhaas, A. Kleinhammes, Y.Y. Jia, Y. Wu, S.B.T. Nguyen, R.S. Ruoff, Synthesis of graphene-based nanosheets via chemical reduction of exfoliated graphite oxide, *Carbon* 45 (2007) 1558–1565.
- [23] J. Shen, T. Li, Y. Long, M. Shi, N. Li, M. Ye, One-step solid state preparation of reduced graphene oxide, *Carbon* 50 (2012) 2134–2140.
- [24] H.L. Wang, J.T. Robinson, X.L. Li, H.J. Dai, Solvothermal reduction of chemically exfoliated graphene sheets, *J. Am. Chem. Soc.* 131 (2009) 9910–9911.
- [25] A. Das, S. Pisana, B. Chakraborty, S. Piscanec, S.K. Saha, U.V. Waghmare, K.S. Novoselov, H.R. Krishnamurthy, A.K. Geim, A.C. Ferrari, Monitoring dopants by Raman scattering in an electrochemically top-gated graphene transistor, *Nature Nanotechnol.* 3 (2008) 210–215.
- [26] C. Nethravathi, B. Viswanath, C. Shivakumara, N. Mahadevaiah, M. Rajamathi, The production of smectite clay/graphene composites through delamination and co-stacking, *Carbon* 46 (2008) 1773–1781.
- [27] H.K. Jeong, Y.P. Lee, R.J.W.E. Lahaye, M.H. Park, K.H. An, I.J. Kim, C.W. Yang, C.Y. Park, R.S. Ruoff, Y.H. Lee, Evidence of graphitic AB stacking order of graphite oxides, *J. Am. Chem. Soc.* 130 (2008) 1362–1366.
- [28] Y.L. Chen, Z.A. Hu, Y.Q. Chang, H.W. Wang, Z.Y. Zhang, Y.Y. Yang, H.Y. Wu, Zinc oxide/reduced graphene oxide composites and electrochemical capacitance enhanced by homogeneous incorporation of reduced graphene oxide sheets in zinc oxide matrix, *J. Phys. Chem., C* 115 (2011) 2563–2571.
- [29] S. Hongqi, F. Xiaohui, W. Shaobin, H.A. Ming, M.O. Tade, Combination of adsorption, photochemical and photocatalytic degradation of phenol solution over supported zinc oxide: Effects of support and sulphate oxidant, *Chem. Eng. J.* 170 (2011) 270–277.
- [30] P. Wang, B. Huang, Z. Lou, X. Zhang, X. Qin, Y. Dai, Z. Zheng, X. Wang, Synthesis of highly efficient Ag@AgCl plasmonic photocatalysts with various structures, *Chem. Eur. J.* 16 (2010) 538–544.
- [31] X. Hui, L. Huaming, X. Jiexiang, Y. sheng, L. Zhijun, L. Ling, X. Li, One-pot synthesis of visible light driven plasmonic photocatalyst Ag/AgCl in ionic liquid, *Chem. Comm.* 3 (2011) 22–29.
- [32] J.F. Shen, M. Shi, N. Li, B. Yan, H.W. Ma, Y.Z. Hu, M.X. Ye, Facile synthesis and application of Ag-chemically converted graphene nanocomposite, *Nano Res.* 3 (2010) 339–349.
- [33] Y. Si, E.T. Samulski, Exfoliated graphene separated by platinum nanoparticles, *Chem. Mater.* 20 (2008) 6792–6797.
- [34] B.F. Machado, P. Serp, Graphene-based materials for catalysis, *Catal. Sci. Technol.* 2 (2011) 54–75.
- [35] D. Yang, L. Zhou, L. Chen, B. Zhao, J. Zhang, C. Li, Chemically modified graphene oxides as a hole transport layer in organic solar cells, *Chem. Commun.* 48 (2012) 8078–8080.
- [36] G. Luo, X. Jiang, M. Li, Q. Shen, L. Zhang, H. Yu, Facile fabrication and enhanced photocatalytic performance of Ag/AgCl/rGO heterostructure photocatalyst, *ACS Appl. Mater. Interface* 5 (2013) 2162–2168.
- [37] P. Wang, B. Huang, X. Qin, X. Zhang, Y. Dai, J. Wei, M.H. Whangbo, Ag@AgCl: A highly efficient and stable photocatalyst active under visible light, *Angew. Chem. Int. Ed.* 47 (2008) 7931–7933.
- [38] J. Yu, G. Dai, B. Huang, Fabrication and characterization of visible-light-driven plasmonic photocatalyst Ag/AgCl/TiO₂ nanotube arrays, *J. Phys. Chem. C* 113 (2009) 16394–16401.
- [39] R.C. Pawar, J.S. Shaikh, S.S. Suryavanshi, P.S. Patil, Growth of ZnO nanodisk, nanospindles and nanoflowers for gas sensor: pH dependency, *Appl. Phys.* 12 (2012) 778–783.
- [40] H. Zhang, X.J. Lv, Y.M. Li, Y. Wang, J.H. Li, P25-graphene composite as a high performance photocatalyst, *ACS Nano* 4 (2010) 380–386.
- [41] Z. Liu, Q. Liu, Y. Huang, Y. Ma, S. Yin, X. Zhang, W. Sun, Y. Chen, Organic photovoltaic devices based on a novel acceptor material: Graphene, *Adv. Mater.* 20 (2008) 3924–3930.
- [42] S.M. Lam, J.C. Sin, A.Z. Abdullah, A.R. Mohamed, Degradation of wastewaters containing organic dyes photocatalysed by zinc oxide: A review, *Desalin. Water Treat.* 41 (2012) 131–169.
- [43] M. Zhang, Q. Wang, C.C. Chen, L. Zang, W.H. Ma, J.C. Zhao, Oxygen atom transfer in the photocatalytic oxidation of alcohols by TiO₂: Oxygen isotope studies, *Angew. Chem. Int. Ed.* 48 (2009) 6081–6084.
- [44] B. Li, T. Liu, Y. Wang, Z. Wang, ZnO/graphene-oxide nanocomposite with remarkably enhanced visible-light-driven photocatalytic performance, *J. Coll. Inter. Sci.* 377 (2012) 114–121.
- [45] J.C. Liu, H.G. Bai, Y.G. Wang, Z.Y. Liu, X.W. Zhang, D.D. Sun, Self-assembling TiO₂ nanorods on large graphene oxide sheets at a two-phase interface and their anti-recombination in photocatalytic applications, *Adv. Funct. Mater.* 20 (2010) 4175–4181.